CrossMark

# Tuning of magnetism in DyMn$_{1-x}$Fe$_x$O$_3$ (x < 0.1) system by iron substitution

Matúš Mihalik[a,*], Marián Mihalik[a], Mária Zentková[a], Klára Uhlířová[b], Marie Kratochvílová[b], Magdalena Fitta[c], Pedro A. Quintero[d], Mark W. Meisel[d]

[a] Department of Magnetism, Institute of Experimental Physics SAS, Košice, Slovak Republic
[b] Department of Condensed Matter Physics, Faculty of Mathematics and Physics, Charles University, Prague, Czech Republic
[c] Institute of Nuclear Physics, Polish Academy of Sciences, Kraków, Poland
[d] Department of Physics and NHMFL, University of Florida, Gainesville, FL, USA

## ARTICLE INFO

## ABSTRACT

The effect of Fe doping on the magnetism of DyMn$_{1-x}$Fe$_x$O$_3$ ($x < 0.1$) single crystals is reported. Specifically, $T_N$ of the Mn sublattice decreases from 38 K ($x = 0$) to 33 K ($x = 0.1$), $T_S = 17.9$ K ($x = 0$) connected with the transition of Mn-spins into the cycloidal magnetic phase decreases to 15.9 K ($x = 0.01$) and vanishes for higher $x$ concentrations, while the ordering temperature of the Dy sublattice varies between 5.9 K ($x = 0.01$) and 4.1 K ($x = 0.02$). These results indicate the ground state magnetic structure of DyMnO$_3$ can be destabilized, and the multiferroicity is completely suppressed by very low Fe doping. Similar effects were previously observed in the multiferroic TbMn$_{1-x}$Fe$_x$O$_3$ system.

## 1. Introduction

The discussion about DyMn$_{1-x}$Fe$_x$O$_3$ ($x < 0.1$) begins with the parent compound ($x = 0$), which orders magnetically below $T_N = 41$ K where the Mn-spins form a longitudinal spin density wave that propagates along the $c$-direction [1]. This structure changes to a cycloidal phase below $T_S = 18$ K, while a ferroelectric phase exists below this temperature [1]. The independent magnetic ordering of the Dy sublattice appears at $T_1 \sim 6.5$ K [1,2], but below 15 K, the Dy-spins begin to polarize and to form the same magnetic structure as the Mn sublattice [3]. The cycloidal Mn-spin structure, with the antisymmetric Dzyaloshinskii-Moriya interaction, is the driving force for the ferro-electric order and the magnetic frustration is the origin of the multi-ferroicity [4]. This frustration can be tuned by modifications of exchange interactions induced, for example, by substitution. The iron substitution has an advantage of good solubility, which allows synthesis of DyMn$_{1-x}$Fe$_x$O$_3$ substitutional solid solutions for the whole concentration range $0 \leq x \leq 1$ [5]. Furthermore, DyFeO$_3$ crystallizes in the orthorhombic crystal structure and DyMnO$_3$ can accommodate the same crystal structure [5,6], which is advantageous for the Mn-Fe substitution. Since the Mn$^{3+}$ ion is Jahn-Teller (JT) active, while the Fe$^{3+}$ ion is not, this substitution directly affects the JT distortion, thereby leading to changes of the magnetic frustration. As a consequence, the magnetism and multiferroicity of the system can be tuned by this substitution.

In the case of TbMn$_{1-x}$Fe$_x$O$_3$, the destabilization of the magnetic cycloidal phase was observed for concentrations $x < 0.05$ [7], and the reduction of the magnetic phase is connected with the simultaneous suppression of the ferroelectric phase [8]. Extrapolating from TbMn$_{1-x}$Fe$_x$O$_3$, one can posit that small substitution of Mn with Fe in the DyMnO$_3$ parent compound will lead to the reduction of the cycloidal magnetic phase and hence to the suppression of the multiferroicity in this system. In order to verify this conjecture, single crystals of DyMn$_{1-x}$Fe$_x$O$_3$, where $x = 0.00, 0.01, 0.02, 0.05, 0.1$, were prepared, and the crystallographic, thermal, and magnetic properties of these compounds were characterized. Herein, the evolution of the magnetic phases with respect to the iron doping is determined and the role of the magnetocrystalline anisotropy is explored.

## 2. Sample preparation and experimental details

Single crystals were prepared by the floating zone method in a 4-mirror optical furnace (type: FZ-T-4000 from Crystal Systems corporation). As starting materials, we used MnO$_2$ (purity 3 N, supplier: Alpha Aesar), Dy$_2$O$_3$ (purity 3 N, supplier: Sigma Aldrich) and Fe$_2$O$_3$ (purity 2 N, supplier: Sigma Aldrich). The starting materials were mixed in a Dy:Mn:Fe stoichiometric ratio as intended for the final compound. Subsequently the powders were cold pressed into rods and sintered at

1100 °C for 8–12 h in air. The parameters of crystal growth were as follows: rotation of both, upper and lower shafts, 15 rpm; pulling speed 5 mm/h; and the crystal growth was performed in an air atmosphere with ambient pressure. The quality and the alignment of the grown single crystals was checked by the Laue method.

X-ray powder diffraction was conducted on samples powdered from the grown ingots and with a X'PERT PRO diffractometer (PANalytical) using Cu K$_{\alpha1,\alpha2}$, doublet radiation and standard Bragg-Brentano geometry. Powder data were treated using Rietveld method implemented in *FullProf* software [9].

Magnetization ($M$), susceptibility ($\chi$), and AC susceptibility ($\chi_{AC}$) measurements were performed on two SQUID magnetometers, MPMS-XL7 and MPMS3 (both from Quantum Design), in the temperature range 2–380 K, and in applied magnetic fields up to 7 T. The samples were either fixed in the plastic straws (MPMS-XL7), or glued by GE varnish on a glass cylinder which was inserted into brass holder (MPMS3). Typical masses of the samples were between 6 and 11 mg.

Molar heat capacity ($C_P$) was measured by the relaxation method on a PPMS apparatus (Quantum Design) in the temperature range 2–220 K. For these measurements, not oriented pieces of single crystals with typical masses between 7 and 15 mg were used.

## 3. Results and discussion

### 3.1. Crystallography

The DyMnO$_3$ compound crystallizes either in orthorhombic (GdFeO$_3$ structural type) or close-packed hexagonal structures, depending on the preparation process; orthorhombic structure – for oxygen atmosphere, hexagonal structure – for argon atmosphere [6]. In our case, all samples were found to be orthorhombic in agreement with the synthesis conditions and the structure can be described using the *Pnma* space group. This notation is used throughout this paper. Since this orthorhombically distorted crystal structure is derived from the original cubic CaTiO$_3$ perovskite by applying $a^+a^-a^-$ tilt according to Glazer's notation [10], it is convenient to introduce the pseudocubic parameters which, in fact, show the degree of distortion of the original cubic cell:

$$a_{pc} = \frac{a}{\sqrt{2}}; b_{pc} = \frac{b}{2}; c_{pc} = \frac{c}{\sqrt{2}}$$

where $a$, $b$, and $c$ are the orthorhombic lattice parameters. The pseudocubic lattice parameters for the studied compounds are plotted in Fig. 1. Our data change linearly with iron content and nicely fill the gaps in the data published by Chiang et al. [5] (We remind that Chiang et al. [5] describes the system using *Pbnm* notation, while we use description in *Pnma* notation of the space group.). At this point, we can conclude that there is no change in the crystallographic symmetry
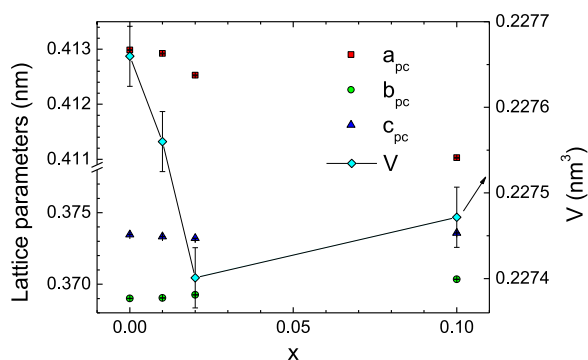


**Fig. 1.** Lattice parameters for DyMn$_{1-x}$Fe$_x$O$_3$; x ≤ 0.1. Note that due to symmetry consideration, the volume of the orthorhombic unit cell is 4 times the volume of the original (non-distorted) cubic cell.
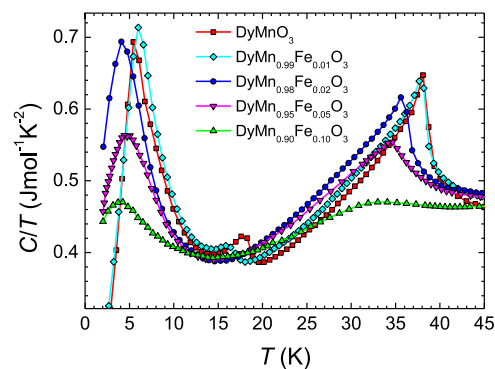


**Fig. 2.** Specific heat of DyMn$_{1-x}$Fe$_x$O$_3$ compounds measured at low temperatures, in all cases with decreasing temperature. The full temperature range data are presented in supplementary Fig. SM1.

induced by Fe doping for iron concentrations lower than 10%. However $a_{pc}$:$b_{pc}$:$c_{pc}$ ratio changes, so the changes in the magnetic structure (see below) can be directly ascribed to the lifting of the JT distortion.
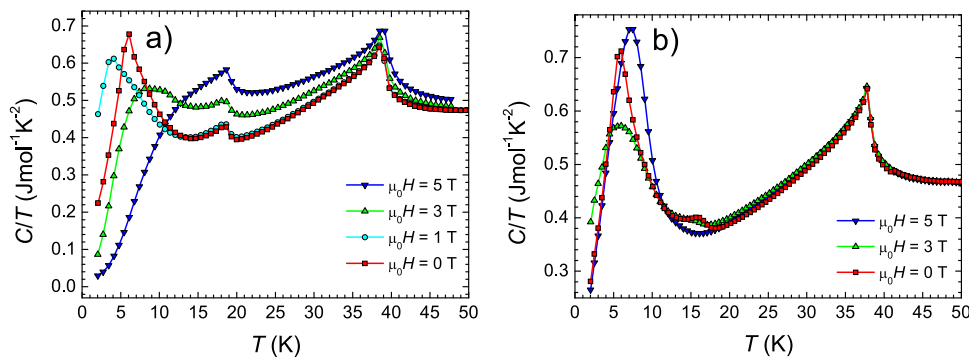
### 3.2. Specific heat

The low temperature details of specific heat data, Fig. 2, show a distinct peak at T$_N$, which shifts almost linearly from 38.1(3) K for parent compound DyMnO$_3$ to 37.7(3), 35.9(3), and 34.7(3) K for $x$ = 0.01, 0.02, and 0.05, respectively. This peak evolves into a broad bump, with maximum at 33(1) K, when $x$ = 0.1. This observation can be considered as a hint that the original magnetic structure is destabilized by Fe doping and that the Mn-O-Fe superexchange interaction either does not exist or is much weaker than the Mn-O-Mn superexchange interaction. The peak connected with T$_S$ shifts from 17.9(3) K for $x$ = 0 to 15.9(3) K for $x$ = 0.01 and vanishes for higher $x$ concentrations. The disappearance of this peak indicates the cycloidal phase is absent. This result is reminiscent of the properties of TbMn$_{1-x}$Fe$_x$O$_3$, where the absence of the cycloidal phase related to the disappearance of ferroelectricity was observed for $x$ < 0.05 [7].

At low temperatures, a broad bump was observed for all concentrations, with maximum at 5.5(3) K, 5.9(3) K, 4.1(5) K, 4.7(2) K, and 4.3(4) K for $x$ = 0, 0.01, 0.02, 0.05, and 0.1, respectively. The similar bump was observed for DyMnO$_3$ at 5 K and was ascribed to ordering of Dy sublattice [11]. Such a bump is typical also for TbMn$_{1-x}$Fe$_x$O$_3$ system [7,12] and was ascribed to the ordering of Tb sublattice. Additionally, specific heat measured in applied magnetic field (Fig. 3) clearly shows that this bump reacts on the magnetic field, as demonstrated for DyMnO$_3$, Fig. 3a), and DyMn$_{0.99}$Fe$_{0.01}$O$_3$, Fig. 3b), so it is of magnetic origin. For that reasons we ascribe this feature to the ordering of Dy sublattice in entire DyMn$_{1-x}$Fe$_x$O$_3$ ($x$ ≤ 0.1) system. The feature is sharpest for $x$ = 0, but even for this concentration it cannot be considered as first, or second order phase transition. This is most likely connected with the fact that Dy ions polarize already below 15 K [3], implicating that the transition at T$_1$ is of higher order. The broadening of the bump for $x$ > 0 can be ascribed to the structural disorder in the system caused by introducing of Fe ions. The position of the bump first shift to lower temperatures for smaller magnetic field, Fig. 3, but shifts to higher temperatures and broadens at sufficiently high magnetic fields. This may be explained by the antiferromagnetic ground state of Dy-sublattice, but subsequent metamagnetic phase transition in applied magnetic field into an induced ferromagnetic state takes place. Such a scenario is in agreement with magnetic measurements presented below.

### 3.3. Magnetic measurements

Magnetic measurements were performed on the samples with $x$ = 0, 0.01, and 0.02. The inverse susceptibility along all three main crystal-

**Fig. 3.** Specific heat of a) $DyMnO_3$ measured with decreasing temperature and b) $DyMn_{0.99}Fe_{0.01}O_3$ measured with increasing temperature and in applied magnetic field up to 5 T.
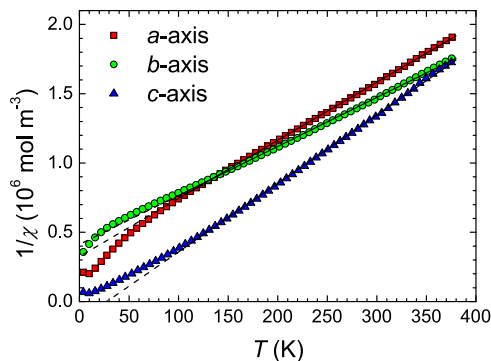


**Fig. 4.** Representative data of inverse susceptibility ($DyMn_{0.98}Fe_{0.02}O_3$ compound) measured in applied field $\mu_0 H = 0.1$ T. Lines represent the best fit due to Curie-Weiss law. Data measured for other iron concentrations are plotted in Supplementary Fig. SM2.

**Table 1**
The results of Curie-Weiss fit as described in the text.

| x | axis | fitting interval (K) | $\theta_P$ (K) | $\mu_{eff}$ ($\mu_B$) |
|---|------|---------------------|----------------|----------------------|
| 0 | a | 100 – 300 | −75.8(1) | 11.7(1) |
| | b | 100 – 300 | −100(1) | 12.3(1) |
| | c | 100 – 300 | 19.2(4) | 10.8(1) |
| 0.01 | a | 100 – 300 | −75.7(3) | 11.7(1) |
| | b | 100 – 300 | −99.7(3) | 13.2(1) |
| | c | 100 – 300 | 20.3(5) | 11.5(1) |
| 0.02 | a | 100 – 380 | −77.4(1) | 12.3(1) |
| | b | 100 – 380 | −117(1) | 13.4(1) |
| | c | 100 – 380 | 27.6(2) | 11.3(1) |
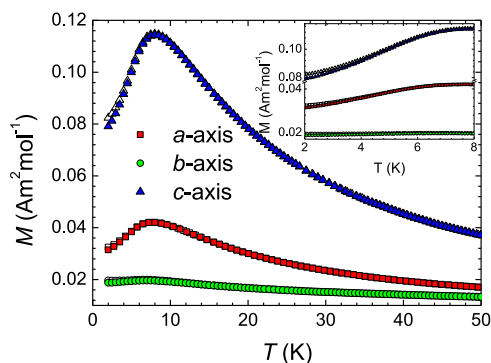


**Fig. 5.** Representative data of ZFC (full symbols) and FC (opened symbols, FC measured in increasing temperature) magnetization curves for $DyMn_{0.98}Fe_{0.02}O_3$ compound measured in applied field $\mu_0 H = 0.01$ T. Data measured for other iron concentrations are plotted in supplementary Fig. SM3.

lographic directions for the studied samples (Fig. 4 and Fig. SM1) is linear at high temperatures. Consequently, these data sets were fit to the Curie-Weiss law

$$\chi = \frac{C}{T - \theta_P}$$

where $\theta_P$ is Weiss temperature and Curie constant $C$ scales with the effective magnetic moment ($\mu_{eff}$) and the results are summarized in Table 1. It is noteworthy that Weiss temperature spans a broad range of values, and this result can be ascribed to the strong magnetocrystalline anisotropy in the system. The effective magnetic moment is roughly within the range $11 - 13$ $\mu_B$. In $DyMn_{1-x}Fe_xO_3$ compounds, one expects that there are three magnetic ions. One can estimate the theoretical effective moment of such a system as:

$$\mu_{eff} = \sqrt{\mu_{eff;Dy}^2 + x\mu_{eff;Fe}^2 + (1-x)\mu_{eff;Mn}^2}$$

where the terms on the right side of the equation represent the effective moments of individual magnetic ions. Using $\mu_{eff;Dy} = 10.63$ $\mu_B$ (theoretical value for 3+ valence), $\mu_{eff;Fe} = 5.92$ $\mu_B$ ($Fe^{3+}$ ion in a high spin state), and $\mu_{eff;Mn} = 4.9$ $\mu_B$ ($Mn^{3+}$ ion in a high spin state), $\mu_{eff} \approx 11.7$ $\mu_B$, with the exact value depending on $x$. Taking into account the anisotropy of the system, the experimentally determined effective moment is close to the theoretically calculated one.

The anomalously high magnetic moment of the Mn sublattice in $DyMnO_3$ below $T_S$ was explained by asserting that, at $T_S$, the Dy spins polarize to the same magnetic structure as the Mn sublattice, which is apparently the effect of the magnetism of the Mn sublattice [3]. On further cooling, the Dy sublattice orders independently from Mn sublattice at $T_1$, however, this ordering changes the propagation vector of the Mn sublattice from (0.36 1 0) to (0.39 1 0) [13]. Subsequently when warming, the propagation vector of the Mn sublattice does not jump back to its original value at $T_1$, but instead undergoes a smooth transition, reaching its original value only close to $T_N$ [13]. This interpretation implies that the magnetic structure is very hysteretic, and consequently, the FC curves were measured in both increasing and decreasing temperature modes. The ZFC-FC curves, when FC data were measured with increasing temperature, exhibit no anomalies at $T_N$ and $T_S$ (Fig. 5 and Supplementary Fig. SM3). However, all curves bifurcate below 10 K, i.e. around the ordering of Dy sublattice. Similar effects were already observed with $DyMnO_3$ [5,11]. It is noteworthy that the ZFC-FC curves measured for different crystallographic directions do not bifurcate all at the same temperature, but within some temperature interval (see Fig. 6 and Fig. SM4). These results directly show the temperature range of irreversibility processes, which are sensitive to the applied magnetic field. In addition, this sensitivity to the direction of the applied magnetic field might be the reason why, in the case of $DyMnO_3$, $T_1$ is reported to be between 5 K and 10 K [1–3,11,13]. The ZFC curve measured during cooling bifurcates from the FC curve at a temperature close to $T_S$ for magnetic field applied along the $b$-axis [Fig. 6b)]. This observation is another hint of the strong magnetic hysteresis in this system.

In the case of AC susceptibility, no special features were detected at $T_N$ and $T_S$ (Fig. 7 and Supplementary Fig. SM5). Only a very broad maximum was noticed around 10 K, 9.5 K, and 8 K for $x = 0$, 0.01, and
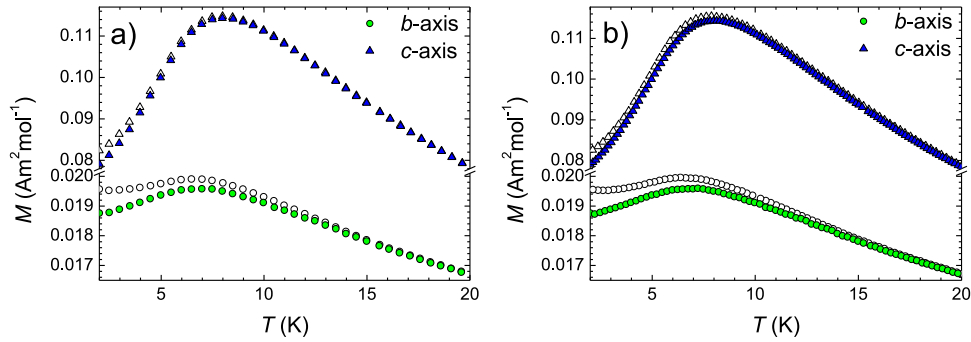
**Fig. 6.** ZFC (full symbols) and FC (opened symbols) magnetization curves for $DyMn_{0.98}Fe_{0.02}O_3$ compound measured in applied field $\mu_0H = 0.01$ T. a) FC curve measured with increasing temperature; b) FC curve measured with decreasing temperature. The remaining data for a-axis are plotted in Fig. SM4.
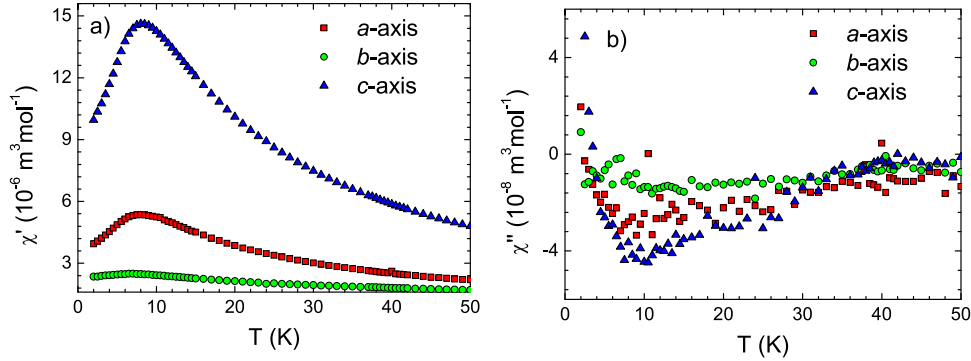


**Fig. 7.** Representative data of AC susceptibility for $DyMn_{0.98}Fe_{0.02}O_3$ compound measured with applied frequency of 333 Hz. a) the real part b) the imaginary part of AC susceptibility. Data measured for other iron concentrations are plotted in Supplementary Fig. SM5.
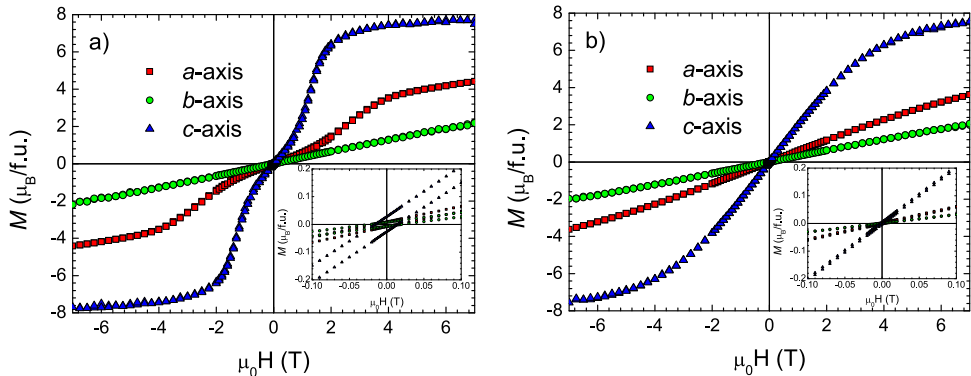


**Fig. 8.** Representative magnetization curves for $DyMn_{0.98}Fe_{0.02}O_3$ compound measured at temperature a) 2 K; b) 15 K. Inserts visualize the low magnetic field region of $\mu(\mu_0H)$. Data for T = 25 K are plotted in Supplementary Fig. SM6. Data measured for other iron concentrations are plotted in Supplementary Fig. SM7.

0.02, respectively, and all of these effects are frequency-independent up to 333 Hz. These effects are similar to these already published on $DyMnO_3$ [11] and we assign them to the magnetism of Dy sublattice.

As presented in previous paragraphs, the characteristic temperatures $T_N$ or $T_S$, which are directly connected with the magnetism of Mn sublattice, cannot be detected by either by magnetization or AC susceptibility measurements. In order to obtain more complex magnetic characterization of our samples, a series of magnetization isotherms $M(\mu_0H)$ were collected (Fig. 8 and Supplementary Fig. SM7). These isotherms revealed that the magnetic moments lie in the $ac$ plane and the $b$-axis is the hard magnetization axis. In all instances at 2 K, metamagnetic steps were observed at 2.75 T for the $a$-axis and at 1 T for the $c$-axis. In addition, all $M(\mu_0H)$ curves measured at 2 K exhibit very small hysteresis with coercive field values of 0.06 T, 0.04 T, and 0.015 T for $x = 0$, 0.01, and 0.02, regardless the crystallographic direction along which the $M(\mu_0H)$ curve was measured. When the temperature is increased to 15 K, metamagnetic steps, as well as magnetic hysteresis, are no longer detected, Fig. 8b), SM6, and SM7.

Since 15 K is lower than $T_S$ for $x = 0$ and 0.01 and in case of $x = 0.02$ there was observed no phase transition below $T_N$, we conclude that both the metamagnetic steps and the small magnetic hysteresis are direct consequences of the magnetic ordering of the Dy sublattice. The $M(\mu_0H)$ curves measured at 15 K and 25 K have qualitatively the same character, only the saturated magnetization for 25 K curve is lower than in case of 15 K curve. This reduction is understandable, since all $M(\mu_0H)$ curves were measured after first cooling to base temperature and then acquiring data during warming. As a result of this protocol, the $M(\mu_0H)$ curves were acquired during the smooth magnetic transition of the Mn sublattice [13].

## 4. Conclusions

The crystallographic, specific heat, and magnetic data for $DyMn_{1-x}Fe_xO_3$ ($x < 0.1$) single crystals have been studied with the aim to probe the response of magnetism and multiferroicity to iron doping. The data reveal that the Néel temperature is suppressed with iron doping over

the entire concentration interval studied in this work. In addition, the iron destabilizes the ferroelectric phase, and by $x = 0.02$, the doping leads to the complete suppression of this phase. From the magnetic point of view for all cases, the magnetic moments lie in the *ac* plane, while the *b*-axis is the hard magnetization axis of the system.

## Acknowledgment

## Appendix A. Supporting information

Supplementary data associated with this article can be found in the online version at doi:10.1016/j.physb.2017.10.037.

## References

[1] T. Kimura, G. Lawes, T. Goto, Y. Tokura, A.P. Ramirez, Phys. Rev. B 71 (2005) 224425.
[2] T. Kimura, Y. Tokura, J. Phys.: Condens. Matter 20 (2008) 434204.
[3] O. Prokhnenko, R. Feyerherm, E. Dudzik, S. Landsgesell, N. Aliouane, L.C. Chapon, D.N. Argyriou, Phys. Rev. Let. 98 (2007) 057206.
[4] S.-W. Cheong, M. Mostovoy, Nat. Mater. 6 (2007) 13.
[5] F.-K. Chiang, M.-W. Chu, F.C. Chou, H.T. Jeng, H.S. Sheu, F.R. Chen, C.H. Chen, Phys. Rev. B 83 (2011) 245105.
[6] S. Remsen, B. Dabrowski, O. Chmaissem, J. Mais, A. Szewczyk, J. Sol. Stat. Chem. 184 (2011) 2306–2314.
[7] M. Mihalik jr., M. Mihalik, Z. Jagličić, R. Vilarinho, J. Agostinho Moreira, E. Queiros, P.B. Tavares, A. Almeida, M. Zentková, Phys. B 506 (2017) 163.
[8] R. Vilarinho, E. Queirós, D.J. Passos, D.A. Mota, P.B. Tavares, M. Mihalik jr., M. Zentková, M. Mihalik, A. Almeida, J. Agostinho Moreira, J. Magn. Magn. Mater. 439 (2017) 167–172.
[9] J.R. Carvajal, Phys. B 192 (1993) 55–69.
[10] A.M. Glazer, Acta Cryst. B 28 (1972) 3384–3392.
[11] S. Harikrishnan, S. Rößler, C.M. Naveen Kumar, H.L. Bhat, U.K. Rößler, S. Wirth, F. Steglich, S. Elizabeth, J. Phys.: Condens. Matter 21 (2009) 096002.
[12] D. O'Flynn, M.R. Lees, G. Balakrishnan, J. Phys.: Condens. Matter 26 (2014) 256002.
[13] T. Finger, K. Binder, Y. Sidis, A. Maljuk, D.N. Argyriou, M. Braden, Phys. Rev. B 90 (2014) 224418.